1 2 3	Including the Effects of Subsurface Currents on Buoyant Particles in Lagrangian Particle Tracking Models: Model Development and its Application to the Study of Riverborne Plastics over the Louisiana/Texas Shelf
4	
5	Jun-Hong Liang <sup>1</sup> , Jinliang Liu <sup>2</sup> , Mark Benfield <sup>1</sup> , Dubravko Justic <sup>1</sup> , Daniel Holstein <sup>1</sup> , Bingqing
6	Liu <sup>3</sup> , Robert Hetland <sup>4*</sup> , Daijiro Kobashi <sup>4</sup> , Changming Dong <sup>5</sup> , Weiyuan Dong <sup>1</sup>
7	
8	<sup>1</sup> Louisiana State University, Baton Rouge, LA, USA
9	<sup>2</sup> University of Cambridge, Cambridge, UK
10	<sup>3</sup> Water Institute of the Gulf, Baton Rouge, LA, USA
11	<sup>4</sup> Texas A&M University, College Station, TX, USA
12	<sup>5</sup> Nanjing University of Information and Technology, Nanjing, China
13	
14	
15	
16	
17	
18	
19	
20	
21	
22	
	Corresponding outhor: Jun Hong Liong (iliang also odu) Department of Oceanography and
23 24	Corresponding author: Jun-Hong Liang ( <u>jliang@lsu.edu</u> ), Department of Oceanography and Coastal Sciences & Center for Computation and Technology, Louisiana State University, Baton
25	Rouge, LA, 70803
26	* Now at Pacific Northwest National Lab, Richland, WA, USA

#### Abstract

27

28

29

30

31 32

33

34

35

36

37

38

39

40

41

42

43

44

45

46

47

We report on the development and implementation of a novel physics-based algorithm that includes the effect of subsurface current on buoyant particles in a Lagrangian particle tracking model, specifically the Larval TRANSport Lagrangian (LTRANS) model. In the upper ocean, the direction and the magnitude of horizontal current change with water depth due to local effects such as the Ekman balance and large-scale influences such as the thermal wind balance. The subsurface current alters both the advection and the dispersion of weakly buoyant particles that could be suspended in the ocean surface boundary layer by turbulence. The transport and fate of riverborne plastics from the Mississippi and Atchafalaya Rivers were examined using a hindcast model solution for the Louisiana and Texas Continental Shelf (LATEX shelf). The model results show that after leaving the river outlets, plastic particles travel on average in a southwestward direction over the LATEX shelf for up to four months, transiting from a few hundred kilometers to more than a thousand kilometers. The pathways and the fate of particles change as a function of the particle size, with smaller particles traveling faster. Also, less buoyant particles transit longer distances over more offshore regions and remain longer on the LATEX shelf. Particle pathways also display strong seasonal cycle associate with the seasonal cycle of circulation on the LATEX shelf. The model results further reveal that more than 50% of the plastic particles delivered by the Mississippi and Atchafalaya Rivers reach the land boundary of the LATEX shelf, and more than 18% of those reach the land boundary west of Louisiana including Texas and portions of Mexico. This modeling framework can be used to study transport of other positively buoyant particulate materials in the ocean, such as spilled oil and plankton.

48

49

50

51

52

53

54

55

56

#### 1. Introduction

Plastic debris has emerged as one of the major pollutants in the oceans and a growing concern and threat to the ocean environment and marine organisms [e.g., Andrady 2011, Law 2017]. Plastic concentrations appear to be increasing in some, if not all ocean basins [e.g. Ostle et al. 2019; Wilcox et al. 2020]. Plastic debris in the ocean is generated by various human activities and enters the ocean along hotspots such as ship tracks, beaches and ocean platforms [e.g., Kershaw et al. 2011]. In addition, plastic debris introduced into inland aquatic environments reaches the ocean through river outflows. The majority of plastic debris floats and remains close

to the ocean surface due to a lower density than that of seawater. For example, Moret-Ferguson et al. [2010] found that the density of plastic debris in the western north Atlantic Ocean ranges from 808 to 1240 kg m<sup>-3</sup> and has an average value of 965 kg m<sup>-3</sup>. After entering the ocean, plastic debris moves under the combined influence of ocean currents and its own buoyant rising/sinking. It accumulates in the convergence zones of horizontal currents, which are known as ocean garbage patches [e.g., van Sebille et al. 2012; van Sebille et al. 2015]. In the ocean, plastic degrades via physical, chemical, and biological processes [Wayman & Niemann, 2021] and the degradation may take hundreds to thousands of years [Andrady, 2011]. Because of its long life in the ocean, plastic debris can be carried long distances from its source and is now found in all ocean basins and marginal seas.

57

58

59

60

61

62

63

64

65

66

67

68

69

70

71

72

73

74

75

76

77

78

79

80

81

82

83

84

85

86

87

Transport and fate of plastic debris is commonly studied by analyzing surface drifters [e.g., Maximenko et al. 2012; van Sebille et al. 2012] and computer model solutions of particle dispersal [e.g., Lebreton et al. 2012; Wichmann et al. 2019]. In those studies, Lagrangian particles representing plastic debris are advected by pre-saved drifter-derived or simulated current fields. Past studies have largely relied on surface currents since the largest concentration of plastic debris is at the ocean surface. Those studies have been able to reproduce the observed locations of ocean garbage patches [e.g., Lebreton et al. 2012; Maximenko et al. 2012; van Sebille et al. 2012]. However, observations have also shown that plastic debris, particularly microplastics ( $< \sim 5$  mm), does not remain at the ocean surface and substantial amounts of those particles can be mixed into the boundary layer [e.g., Kukulka et al. 2012; Reisser et al. 2015]. Due to the earth's rotation, both the magnitude and the direction of the wind- and wave-driven horizontal currents change with water depth within the ocean surface boundary layer where buoyant plastic debris is located. Furthermore, horizontal currents also change with depth due to larger-scale circulations, such as the thermal wind current in the presence of a horizontal density gradient. Buoyant particles such as plastic debris under the influence of subsurface current moves at different rates and directions from that purely driven by surface currents [e.g., Yang et al. 2015]. In addition to the advective effect of subsurface current, a vertically varying horizontal current also disperses particles that constantly transit across the shear. Using a series of simulations with three simplified representations of vertical mixing and idealized representations of subsurface current effects, Wichmann et al. [2019] demonstrated that subsurface currents alter the large-scale meridional transport of plastic debris and allows more plastic debris to be

transported from low to high latitude regions such as the Arctic region. A more mechanistic representation of subsurface currents has not been tested.

With a combined annual discharge of 730.86 billion m<sup>3</sup> y<sup>-1</sup>, the Mississippi and Atchafalaya Rivers (Fig. 1) drain a catchment with a population of over 100 million people. While major river systems are widely acknowledged as being primary conduits for plastics from land to the sea (Schmidt et al. 2017; van Emmerik and Schwarz, 2019), few estimates of the numerical or mass flux of plastics in the Mississippi are available. Scircle et al., (2020) estimated that 87 to 129 trillion plastic particles (>0.30 μm) were transported daily by the Mississippi River at New Orleans. Toner (2020) estimated a daily flux of 897 million particles (500 to 5000 µm). The orders of magnitude difference between these estimates is likely due to the vastly different size ranges considered and the sample volumes used (1 L versus 10s of cubic meters, respectively). Despite the paucity and range of data on plastic flux in the Mississippi River, it is undoubtedly an important source of plastic debris for the northern Gulf of Mexico (NGoM) (Di Mauro et al. 2017). The transport and fate of riverborne plastics in the NGOM has not been previously studied. While models have explored transport of other positively buoyant particulate materials in this region, such as macroalgae Sargassum [e.g., Zhong et al. 2012], spilled oil [e.g., Liu et al. 2011; Weisberg et al. 2018], and coral larvae [e.g. Davies et al. 2017; Limer et al. 2020] and generic floating particles [e.g., Bracco et al. 2019], neither riverine input of particulate material nor the effect of subsurface current were addressed in those studies. 

The NGoM is characterized by a broad continental shelf (<200 m deep), i.e., the Louisiana-Texas (LATEX) continental shelf, usually defined as inshore of the 100-m isobath, which is tens of kilometers wide (Fig. 1). Over the shelf, wind forcing and ocean circulation exhibit distinct seasonal cycles [Figs. 2a to 2d]. In non-summer months, the primary circulation over the LATEX shelf, called the Louisiana coastal current (LCC), is westward (downcoast) (Fig. 2c), while the LCC reverses its direction and is eastward (upcoast) in summer months (Fig. 2d) [e.g., Wiseman et al. 1997; Hetland and DiMarco 2008]. The seasonal cycle of the LCC is primarily driven by the wind (Figs. 2a and 2b) whose alongshore component has the same seasonal cycle as the coastal currents [e.g., Nowlin et al. 2005]. South of the LCC, the western boundary current of the GoM with a magnitude of around 0.5 m s<sup>-1</sup>, i.e., the Mexican current (MC) [e.g., Zavala-Hidalgo et al. 2003], flow in the opposite direction as the LCC except during summer. The LCC and the MC are important in the pathway and fate of dissolved and particulate materials from the

119 Mississippi and the Atchafalaya rivers, such as dissolved salts [e.g., Morey et al. 2003], inorganic

nutrients [e.g., Justic et al. 2002], dissolved organic matters [e.g., da Silva and Castelao 2018;

Liu et al. 2019], sediments [e.g., Walker et al. 2005] and spilled oil [e.g., Thyng 2019], in the

122 NGOM.

125

128

134

136

137

138

139

142

145

The objectives of this study are threefold: (1) to develop and implement a physics-based

algorithm that includes the effect of subsurface current on buoyant particles in a Lagrangian

particle tracking model; (2) to study the transport and fate of plastics delivered by the Mississippi

and Atchafalaya on the Louisiana-Texas continental shelf; and (3) to assess the importance of

subsurface current on plastic transport in this region. The rest of the paper is organized as follows:

Section 2 describes the algorithm and its implementation. Section 3 introduces the application of

the model to the LATEX shelf; Section 4 discusses simulation results and their relevance to

transport and fate of riverborne plastics; Section 5 is a summary; and the acknowledgement

section contains the access information to the computer code described in the study.

## 2. A Physics-based Algorithm for Including the Effect of Subsurface Currents in

## 133 Lagrangian Particle Models

### 2.1 Formulation and Implementation

Ocean plastics are commonly tracked using Lagrangian particle models, as Lagrangian particle

model avoids the spurious diffusive and dispersive errors inherent to the solutions of Eulerian

material concentration models that are a combination of hyperbolic and parabolic partial

differential equations [e.g., Morton and Mayers 2005]. In most existing Lagrangian tracking

studies of marine plastics, surface currents are used to calculate the location of plastic particles

140 [e.g., Lebreton et al. 2012], i.e.,

$$x(t + \delta t) = x(t) + f(u_{sfc}, \delta t)$$
 (1a)

$$y(t + \delta t) = y(t) + f(u_{sfc}, \delta t)$$
 (1b)

where, t is time,  $\delta t$  is the time step, (x, y) are horizontal locations;  $(u_{sfc}, v_{sfc})$  are the horizontal

velocities at the ocean surface, and  $f(u_{sfc}, \delta t)$  is the time integration scheme. Observations,

however, show that plastic particles, particularly small ones with small buoyant rising speeds,

move up and down rapidly in the ocean surface boundary layer (the upper few to tens of meters)

under the combined influence of turbulent current and their own buoyancy [Kukulka et al. 2012].

Therefore, plastic particle transport is influenced by not only the surface current, but also subsurface currents. Forecasting/hindcasting ocean models are based on the hydrostatic assumption, vertical currents in those models are due to meso- to large-scale circulations (~10<sup>-5</sup> m/s to 10<sup>-6</sup> m/s) and are orders of magnitudes weaker than the vertical currents associated with boundary layer turbulence (~10<sup>-2</sup> cm/s). In fact, the vertical current in forecasting/hindcasting models is so weak that even weakly buoyant particles cannot be suspended. Even for particles of buoyant rising speed comparable to the vertical current in forecasting/hindcasting models, they are not able to move up and down quickly in the ocean surface boundary layer where both the magnitude and direction change drastically with water depth under the combined influence of the earth's rotation, surface and lateral forcings. Therefore, the inability to resolve the rapid vertical turnover of particles in the turbulent ocean surface boundary layer in Lagrangian tracking models leads to inaccurate estimate of horizontal speed and transport of weakly buoyant particles such as microplastics.

To include the effect of subsurface currents for weakly buoyant particles, the calculation of particle location in the LTRANS model, i.e., equation (1), is modified as,

$$x(t + \delta t) = x(t) + f(\bar{u}, \delta t) + x_{sqs}(x, y, t)$$
 (2a)

$$y(t + \delta t) = y(t) + f(\bar{v}, \delta t) + y_{sqs}(x, y, t)$$
 (2b)

where  $(\bar{u}\ \bar{v})$  are the weighted-averaged horizontal velocities in (x, y); and  $x_{sgs}$  and  $y_{sgs}$  are the subgrid-scale (SGS) displacements. The weighted-averaged velocities, i.e.,  $(\bar{u}, \bar{v})$ , are calculated as,

$$\overline{u}(x,y,t) = \langle u(x,y,t)F(x,y,z,t)\rangle/\langle F(x,y,z,t)\rangle$$
 (3a)

$$\bar{v}(x,y,t) = \langle v(x,y,t)F(x,y,z,t)\rangle/\langle F(x,y,z,t)\rangle \tag{3b}$$

Here, the angle bracket denotes the depth average, e.g.,  $\langle u \rangle = \frac{1}{h} \int_{-h}^{0} u \, dz$  with h the boundary layer depth; and F(x, y, z, t) is the mean particle distribution. It is calculated by assuming the distribution is stationary so that the balance between advection by buoyant rising and turbulent diffusion, i.e.,  $w_b F_z = (A_{ks} F_z)_z$  with zero flux at the surface and the base of the ocean surface boundary layer, is achieved,

$$F(x, y, z, t) = Cexp\left(w_b \int_{-h}^{z} \frac{ds}{A_{ks}(x, y, s, t)}\right)$$
(4)

- where C is a constant and is set to ensure  $\langle F \rangle = 1$  in the model for simplicity;  $w_b$  is the rising
- velocity of the particles; and  $A_{ks}(x,y,z)$  is the vertical diffusivity at horizontal location (x,y) and
- 171 depth *z*.
- 172 The subgrid-scale displacement in equation (2) is calculated using the random displacement
- 173 model as [e.g., Griffa 1996],

$$x_{sgs} = (2k_{xx})^{1/2} d\xi (5a)$$

$$y_{sgs} = (2k_{yy})^{1/2}d\xi (5b)$$

- In the above equation,  $d\xi$  is a Gaussian white noise with its variance  $\delta t$ ; and  $k_{xx}$  and  $k_{yy}$  are the
- 175 effective diffusivity calculated as,

$$k_{xx} = -\langle (u - \bar{u})M \rangle \tag{6a}$$

$$k_{vv} = -\langle (v - \bar{v})N \rangle \tag{6b}$$

- where the perturbation particle concentration  $M(x, y, z, t) = F(x, y, z, t) \int_{-h}^{z} \frac{\psi_u(x, y, s, t)}{F(x, y, s, t)A_{kS}(x, y, s, t)} ds$
- and  $N(x, y, z, t) = F(x, y, z, t) \int_{-h}^{z} \frac{\psi_{v}(x, y, s, t)}{F(x, y, s, t) A_{ks}(x, y, s, t)} ds$  with  $\psi_{u}(x, y, z, t) = \int_{-h}^{z} (u(x, y, s, t) u(x, y, z, t)) ds$
- 178  $\bar{u}$ )F(x,y,s,t)ds, and  $\psi_v(x,y,z,t) = \int_{-h}^{z} (v(x,y,s,t) \bar{v})F(x,y,s,t)ds$ . Equation (6) is based
- on fluid dynamical principles, and is derived by applying the multiscale expansions and the
- method of moments on the Fokker-Plank equation for the probability density function of particle
- 181 concentrations. It mechanistically takes into the account of the vertical shear of horizontal
- currents. Detailed derivation can be found in Liang et al. [2018].
- The rationale behind the revised algorithm is that each Lagrangian particle represents numerous
- actual buoyant particles that follow a vertical distribution F(x, y, z, t) determined locally by the
- balanced between turbulent mixing and buoyant rising at its location. The Lagrangian particles
- still move in only the horizontal direction, as the actual particles are still confined in the ocean
- surface boundary layer due to their buoyancy. Instead of being moved around by the surface
- 188 current as in most existing plastic tracking studies, the Lagrangian particles are advected by
- weighted-averaged current  $(\bar{u}, \bar{v})$  and disperse following the effective diffusivity  $(k_{xx}, k_{yy})$ .

In this study, Equations (2) to (6) are implemented in the Larval TRANSport Lagrangian model 190 (LTRANS) [North et al., 2011]. The time advancement follows that in the LTRANS model, i.e., 191 the Runge-Kutta 3<sup>rd</sup> scheme. The LTRANS model is an off-line particle tracking model that is 192 driven by stored current fields from hindcasting/forecasting ocean models. The model has been 193 used for the tracking of a variety of ocean particles such as marine organisms [e.g., North et al. 194 2008] and spilled oil [e.g., North et al. 2011]. The LTRANS model is similar to other Lagrangian 195 particle tracking models [e.g., Paris et al. 2013; Lange and van Sebille, 2017; Delandmeter and 196 van Sebille 2019; Peytavin et al. 2021]. The LTRANS model was selected for this study because 197 it is compatible with outputs using the Regional Ocean Modeling System (ROMS) [e.g., 198 199 Shchepetkin and McWilliams 2005; Haidvogal et al. 2008], namely C-Grid predictions with sigma-coordinates. 200

# 3. Model Application to Riverborne Plastics over the NGOM

201

217

218

219

220

202 To study transport and fate of plastics from the Mississippi and Atchafalaya Rivers, the Texas-Louisiana (TX-LA) hindcast solutions [Zhang et al. 2012b; Kobashi and Hetland, 2020] were 203 204 used to drive the LTRANS model. The TX-LA hindcast solutions were obtained by configuring the ROMS model at a curvilinear grid that covers the continental shelf off the coast of Texas and 205 Louisiana (Fig. 1). The horizontal resolution of the model ranges from about 0.5 km close to the 206 207 coast to approximately 3 km close to the open boundaries. Submesoscale currents are permitted, 208 but are not fully resolved with the finest resolutions, while mesoscale and regional-scale currents 209 are fully resolved in the model solution. Surface boundary conditions were interpolated using the ECMWF's ERA interim data set [Dee et al. 2011], and the lateral boundary conditions were 210 interpolated from the Global Hybrid Coordinate Ocean Model (Glo-HYCOM) [Cummings and 211 Smedstad, 2013, http://www.hycom.org] and Global Mercator (https://marine.copernicus.eu). 212 Other details of the model configuration and extensive validation with observational datasets are 213 214 given in Kobashi and Hetland [2020]. Three-dimensional ocean velocities, temperature, salinity, and eddy viscosity saved at three-hour intervals are inputs to the LTRANS model and are 215 interpolated to the location of the particles. 216

In the hindcast solution, eddy viscosity is diagnosed using the generic length scale (GLS) model [Umlauf and Burchard 2001]. Surface boundary layer depth is not an output of ROMS solutions using the GLS model for vertical mixing, but is needed in the algorithm presented in section 2.1. It is therefore determined using model outputs of density and diffusivity profiles. When surface

forcing is strong, the ocean surface boundary layer is limited by pycnocline and is effectively the mixed layer. When surface forcing is weak, the surface boundary layer could be shallower than the mixed layer. To include both scenarios, the bottom of the boundary layer is defined as the smallest depth where one of the following two criteria is met: (a) the density at the depth is 0.01 kg m<sup>-3</sup> larger than the surface density; or (b) the vertical diffusivity ( $A_{ks}$ ) at the depth is smaller than  $1 \times 10^{-4}$  m<sup>2</sup> s<sup>-1</sup> and the absolute difference of vertical diffusivity from the model element right above is smaller than 1×10<sup>-4</sup> m<sup>2</sup> s<sup>-1</sup>. Surface momentum and buoyancy fluxes together with the profiles of density, diffusivity and horizontal currents were examined for a large number of locations and occurrences and the criteria to identify boundary layer depth is deemed robust. The same criteria could be applied to determine boundary layer depth when other vertical mixing schemes are used. The difference between the horizontal current averaged over the ocean surface boundary layer (OSBL) and the surface current, i.e., the subsurface current effects for neutrally buoyant particles, is shown in Figs. 2(e) and 2(f), and the magnitude and direction of the subgrid-scale effective diffusivity ( $k_{major}$  and  $k_{minor}$ ) for neutrally buoyant particles is shown in Figs. 2(g) and 2(h). The OSBL-averaged current is weaker than the corresponding surface current in regions where the surface current is strong. The difference from the surface current is more than 30% during nonsummer months over most of the domain. In the summer months, the difference in magnitude is smaller, and but is still larger than 5% over most of the domain. The magnitude of the SGS diffusivity is at the order of 10s of m<sup>2</sup>/s. The SGS diffusivity is highly anisotropic, and its direction generally aligns with the along-shore direction. Three groups of simulations are conducted. In the first group of simulations, particles are assumed to float at the surface and represent particles that have a large rising speed (indicated as  $w_b = \infty$  hereafter). This group of simulations is also used to represent traditional plastic trajectory simulations where the effects of subsurface currents are neglected. In the next two groups of simulations, particles are assigned a constant rising speed of 0.5 mm/s and 10 mm/s, respectively. Observations in the North Atlantic Gyre (Fig. 5 of Reisser et al. [2015]) show that the majority of plastic particles have a rising speed between the two values chosen in this study, and those being mixed into the ocean surface boundary layer have a rising speed smaller than 10 mm/s. Depending on the shape and density of plastics, the two rising speeds correspond to plastic

221

222

223

224

225

226

227

228

229

230

231

232

233

234

235

236

237

238

239

240

241

242

243

244

245

246

247

248

249

250

251

particles with a size range of sub-millimeter to tens of millimeters [Reisser et al. 2015]. In each

simulation, a total of 1200 particles are released at three different locations, i.e., the outlets of the Mississippi River (~[28.9°N, 89.45°W)), the Atchafalaya River (~[29.44°N, 91.28°W]), and the Wax Lake Pass (~[29.47°N, 91.45°W]). The particle releases are repeated on the 1st and 16th day of each month from January 2008 to December 2015 and a total of 576 simulations were conducted. A climatology of the trajectory and the fate of plastic particles is established using the 8-year solutions with hourly outputs. The tracking for each particle is conducted until a particle reaches either the open boundaries or the land boundaries of the computational domain. In this study, we consider that a particle "beaches" when it hit the land boundary. It has been observed that buoyant materials that are within hundreds of meters from the land boundary are largely retained in the region and the nearshore water is called sticky water [e.g., Wolanski and Spangol, 2000] or coastal boundary layer [e.g., Nickols et al. 2012]. It was also shown that waves greatly enhance the beaching of oil brought to the nearshore ocean by circulations [Weisberg et al. 2017]. While the model grid next to the land boundary has a resolution of a few hundred meters and does not resolve surf-zone processes, particles that hit the land boundary are considered beached in this study.

### 4. Results

Figure 3 shows the mean paths (lines), and the percentage reaching a location of the domain (heat maps) for particles released from the Mississippi and the Atchafalaya Rivers between 2008 and 2015. Particles from the Atchafalaya River outlet and the Wax Lake outlet is grouped together as from the Atchafalaya particles as both outlets drain the Atchafalaya River. The total transit distance, transit time and average speed are summarized in Fig. 3. Here, the total transit distance is the sum of transit distance using neighboring outputs. The total transit distance is substantially longer than that shown by the mean trajectories in Fig. 2, as particle motions associated with eddies and inertial oscillation are smoothed out in the mean trajectories. The fate locations of the plastic particles in the domain are summarized in Fig. 4. Note that all results in Figs. 2 and 4 assume that particles are released evenly in time. In reality, plastic fluxes from the rivers are not uniform in time, as will be discussed in Section 5.

### 4.1 Simulated Transport and Fate

We will first focus on the climatological trajectory and fate of floating particles ( $w_b = \infty$ ) as those particles are the ones tracked in existing plastics transport models. On average, floating particles

move southwestward after leaving the river outlets (Fig. 3(a) and 3(b)) and their trajectories cover the whole LATEX shelf. Particles from the Mississippi River travel approximately 722 km over ~37 days and those from the Atchafalaya River travel about 455 km over ~34 days (Fig. 4). Mississippi River particles transit through regions further offshore and at a >30% higher speed compared to those from the Atchafalaya River/Wax Lake Outlet, consistent with a previous study showing that the Mississippi River plume is faster than the Atchafalaya River plume [Zhang et al. 2012a]. Around 65% of the Mississippi River particles and about 90% of the Atchafalaya River particles stop (or beach) at the land boundary. Particles that stop at the open boundary may move eastward to other parts of the Gulf with the Mexican Current and some may even leave the Gulf advected with the Loop Current, as is evidenced by the studies of the fate of the river plume water [e.g., Hu et al. 2005; Walker et al. 1994]. It is also possible that some of the particles that stop at the open boundary of the domain re-enter the domain with westward propagating loop current eddies [e.g., Alvera-Azcarate et al. 2009; Liu et al. 2016] and eventually reach the land boundary, particularly the coastline west of Louisiana, including that of Texas and portions of Mexico. The fate of particles that stop at the open boundary can only be evaluated using circulation fields that encompass the whole Gulf of Mexico. The particle beaching statistics presented in this study, therefore, are likely conservative estimates. Only slightly more than 20% of the floating particles from both rivers stop at the coast west of Louisiana. Since the mean surface current in the LATEX is westward, except during summer when the winds can become weakly upwelling favorable, only about 20% of the floating particles stop east of their origins.

#### 4.2 Effect of Subsurface Current

282

283

284

285

286 287

288

289

290

291

292

293

294

295

296

297

298

299

300

301

302

303

304

305

306

307

308

309

310

311

312

Subsurface current alters both the trajectory and the fate of weakly buoyant particles and the effect of subsurface current increases with decreasing buoyant rising speed (Figs. 3, 4, and 5). With decreasing rising speed, particles transit through more offshore regions. For example, for the slowest rising Mississippi River particles ( $w_b = 0.5 \text{ mm/s}$ ), the mean trajectory ends offshore of the 50-m isobath while that of faster-rising Mississippi River particles stop inshore of the 50-m isobath (Fig. 3). They also travel a substantially longer distance and for a significantly longer period before stopping at the boundaries than the faster-rising particles from the same origin. The slowest rising Mississippi River particles on average travel >1185 km over >65 days before reaching the boundaries (Fig. 4). The transit speed is slightly lower for weakly buoyant particles. This is expected as the surface current is stronger when wind and the background current is in

the same direction, as is mostly the case over the region. Slower-rising particles ( $w_b = 0.5 \text{ mm/s}$ ) have a lower chance of stopping at the land boundary than floating and faster-rising particles do (Figs. 5(a) and 5(e)). They have a lower chance of stopping at the land boundary of Louisiana (Figs. 5(b) and 5(f)) but have a higher chance of stopping at the land boundary west of Louisiana (Figs. 5(c) and 5(g)). The zonal fate of the particles is not influenced by the subsurface current

318 (Fig. 5(d) and 5(h)).

313

314

315

316

317

319

320

321

322

323

324

325

326

327

328

329

330

331

332

333

334

335

339

340

341

342

The effect of subsurface current on the fate of particles could be understood by examining a transect of horizontal currents (Fig. 6) that is representative of that in the LATEX shelf. The seasonal cycle of mixed layer depth, the Louisiana coastal current, and the upwelling/downwelling circulation is evident. Inshore of the 100-m isobath, the alongshore current is the strongest near the surface and decreases with depth. The alongshore current is substantially stronger than the cross-shore current. As shown in Zhang et al. [2014], the mean along-shore current is primarily in thermal-wind balance, driven by the strong cross-shore density gradient, particularly in non-summer months. The shore-ward current, largely associated with downwelling circulation, is also surface-intensified. Therefore, slower-rising buoyant particles have a slower shoreward motion and might stay for a longer period in the ocean before beaching. At higher frequencies, the inertial and weather band flows often reverse with depth, creating a two (or more) layer flow; this is in part due to the coastal constraint that confines the depth average cross-shore flow to be small. Particles rising through this strongly sheared flow may enhance particle dispersion in the alongshore direction. The mean vertical shear in the alongshore direction also dominates over that in the cross-shore direction. Therefore, the effective diffusivity is largely in the alongshore direction (Figs. 2e and 2f).

## 4.3 Seasonal Cycle

- Since both the wind and the circulation show a strong seasonal cycle, the trajectory and the fate of riverine particles also exhibit strong seasonal cycles (Figs. 4 and 5). For particles of different rising speeds, the seasonal cycle is qualitatively similar, but quantitatively different.
  - For Mississippi River particles, both the transit distance and transit time are lower in the first half of the year than the second half of the year (Figs. 4a and 4b). Particles released between January and April have a relatively high chance of beaching at the coast of Louisiana (Fig. 5b). During those months, there is a strong surface-intensified shoreward current driven by downwelling

favorable wind and the Louisiana coastal current in the largely alongshore direction is westward. Particles released between May and July have a relatively low probability of beaching and a relatively high probability of stopping east of the river outlet due to the reversal of the Louisiana coastal current. Therefore, particles released during the two seasons travel for a relatively short distance before beaching. Note that the seasonal cycle for beaching at the coast of Louisiana (Fig. 5b) is less evident for weakly buoyant particles ( $w_b = 0.5 \text{ mm/s}$ ) than for strongly buoyant ( $w_b = 10 \text{ mm/s}$ ) and floating particles ( $w_b = \infty$ ). As discussed earlier, weakly buoyant particles are subject to less influence of the shoreward surface-intensified downwelling current because they spend substantial time below the ocean surface. The seasonal cycle for Atchafalaya particles qualitatively similar though less evident than that for Mississippi particles.

## 5. Transport and Fate of Riverborne Plastics over the LATEX shelf

The riverine plastics discharge likely changes over an annual cycle and so the trajectory and fate of plastics are therefore different from the averages shown in Figs. 4 and 5. A climatological plastics discharge from the Mississippi and Atchafalaya rivers has yet to be established. Here, we use an 11-month observation of plastics flux at the Baton Rouge and New Orleans stations of the Mississippi River [Toner, 2020] to represent the seasonal plastics flux from the Mississippi and Atchafalaya rivers (Fig. 7). This is the first observational attempt to quantify plastics flux from the two rivers. The observations were collected with a Manta net at five stations spanning Baton Rouge and New Orleans, Louisiana between day 309 (Nov. 5<sup>th</sup>) of 2016 and day 273 (Sept. 30<sup>th</sup>) of 2017. The count is for plastics between 0.5 and 5 mm (microplastics), although the size and shape distributions of the measured plastics are not established. Therefore, plastic particles of different sizes are assumed to have the same seasonal cycle. Plastics discharge reaches its peak at around May and is the lowest in late fall and winter. The peak of the plastics discharge lags about a month behind the peak in the riverine freshwater discharge [e.g., Martinez-Lopez and Zavala-Hidalgo 2009].

The plastics discharge flux is used to calculate the annual mean statistics for riverine plastics (Table 1). In the calculation, plastics discharge for October that is missing from the observations is linearly interpolated from the rest of the time series. Since plastic flux has its peak in late spring and early summer, the statistics for plastics is influenced more strongly by those months when buoyant particles travel shorter distances, over shorter time periods, at higher speeds, with

fewer particles stopping at the land boundaries, in particular the coast west of Louisiana. On average, Mississippi River plastics travels >600 km over >30 days. Both travel distance and travel time is more than 50% larger for weakly buoyant plastics than for floating plastics. Atchafalaya River plastics travels over a shorter distance than Mississippi River plastics. The difference in travel time is small for floating plastics ( $w_b = \infty$ ) but is more evident for weakly buoyant plastics ( $w_b = 0.5 \text{ mm/s}$ ). At least 50% Mississippi plastics and 80% Atchafalaya plastics stop at the land boundaries of the LATEX shelf. The percentage is likely higher because plastic particles that stop at the open boundary of the domain may be swept into the domain again and eventually reach the land boundary. Subsurface currents move plastics more offshore, as explained in Section 4.2, and the percentage of plastic reaching the land boundary decreases with decreasing rising speed.

# 6. Summary and Future Directions

The major conclusions of the paper are:

- (1) An algorithm that mechanistically includes the effect of subsurface currents on the horizontal movement of buoyant particles is implemented in the Larval TRANSport Lagrangian (LTRANS) model in a dynamically consistent way. The updated LTRANS model is readily run in conjunction with for standard output from the Regional Ocean Modeling System (ROMS) (Sections 2 and 3).
- (2) Buoyant particles from the Mississippi and the Atchafalaya rivers on average move southwestward and cover the LATEX shelf (Section 4).
  - (3) Both the trajectory and fate of weakly buoyant particles are affected by subsurface currents. The slowest rising particles on average travel a longer distance for a longer period at a lower speed. They also are less affected by the surface-intensified downwelling/upwelling currents, showing a weaker seasonal cycle for beaching in the state of Louisiana (Section 4).
  - (4) More than 50% of the Mississippi River plastics and 80% of the Atchafalaya River plastics stop at the land boundaries of the LATEX shelf. The probability of beaching decreases with decreasing buoyant rising speed (Section 5).
- The modeling framework presented here is not only useful for the tracking of marine plastics, it can also be applied for the tracking of other weakly buoyant particulate materials in the ocean,

- such as oil droplets and plankton. While oil slicks float at the ocean surface, they are broken into
- droplets of 10s to 100s of microns after the application of dispersant. Many planktonic organisms
- are also weakly buoyant and have rising speed of a few mm/s or smaller.
- 406 There are still uncertainties associated with the estimate of the trajectory and the fate of
- simulated riverine plastic particles over the LATEX shelf. Those uncertainties could be reduced
- by more accurate plastics flux estimates from the Mississippi and the Atchafalaya Rivers, by
- 409 more realistic representation of plastics dynamics and by the resolving more physics in the ocean
- 410 circulation fields.
- 411 Comprehensive, long-term observations of plastics in the Mississippi and Atchafalaya Rivers,
- 412 including particle properties, are needed to better constrain the model. Extreme plastics pulse
- 413 events, such as the nurdle spill event near New Orleans in August 2020
- 414 (https://www.nola.com/news/environment/article b4fba760-e18d-11ea-9b0b-
- 415 <u>b3a2123cf48b.html</u>), are likely to have a substantial impact on plastics concentration over the
- 416 LATEX shelf.
- While the rising speed of a Lagrangian particle is constant in the simulation, the rising speed of
- 418 plastic particles is variable in the realistic ocean. It could vary due to the change in seawater
- density that is significant from river outflows to the open ocean. It could also change due to the
- aggregation of plastic particles with negatively buoyant particulate materials of either organic or
- 421 mineral origins [e.g. van Sebille et al. 2020]. Since rising speed determines the importance of
- particle speed and direction, change in rising speed during their transport influence the pathway
- 423 and destine of plastics.
- 424 Regarding the physics of the circulation field, the biggest uncertainty may be associated with the
- effects of ocean surface gravity waves that are not included in the hindcast solution for the
- 426 LATEX shelf. The inclusion of ocean surface gravity waves could alter the trajectories of
- buoyant particles in the following two ways. First, waves alter the vertical mixing in the upper
- ocean. Waves can enhance vertical mixing by the generation of Langmuir circulation [e.g.,
- D'Asaro 2014] or by the wave orbital velocities [e.g., Dai et al. 2010; DiBenedetto 2020]. Waves
- can also suppress vertical mixing when it is in the opposite direction of near-surface current [e.g.,
- van Roekel et al. 2012; McWilliams et al. 2014]. The effect of waves on vertical mixing is
- important in many regions of the global ocean [Li et al. 2019] including over the Gulf of Mexico

[e.g., Ali et al. 2019]. Vertical mixing controls the distribution of buoyant particles including plastics in the ocean surface boundary layer [e.g., Chor et al. 2018; Kukulka and Brunner 2015; Liang et al. 2012] and therefore the effect of subsurface currents on plastics. In addition to the effect of waves, recent studies also demonstrate that the northward component of the earth's rotation [e.g., Liu et al. 2018] and submesoscale currents [e.g., Hamlington et al. 2014; Yuan and Liang et al. 2021] could further alter vertical mixing and thereby the effect of subsurface currents on plastics. Secondly, the wave-induced Stokes drift is important in the transport of floating materials such as plastics. Ocean surface gravity waves and Stokes drift can be in very different directions from the wind and the current over the world's ocean [e.g., Hanley et al. 2010], including over the Gulf of Mexico and the LATEX shelf [Abolfazli et al. 2020]. In the open ocean, Stokes drift has been shown to influence the large-scale transport of plastics [e.g., Fraser et al. 2018; Dobler et al. 2019] when only surface current is considered. In the coastal ocean, waves refract due to bottom topography and propagate perpendicular towards the shoreline when approaching the coastline. It was shown that Stokes drift is responsible for oil beaching in the northern Gulf beaches [Weisberg et al. 2017]. The effect of Stokes drift on plastic propagation over the LATEX shelf remains to be investigated.

Another important dynamical process not fully resolved in the circulation field is submesoscale currents. With a spatial resolution of 500 m and an archive interval of 3 hours, the model output in this study marginally resolves submesoscale currents. Sensitivity studies using 6-hourly ROMS solutions were also conducted. The particle solutions using 3-hourly and 6-hourly ROMS outputs are qualitatively the same, though as expected, slightly quantitatively different. In a recent study that examines the sensitivity of Lagrangian particle solutions to the resolution of archived hydrodynamic solutions, Dauhajre et al. [2019] showed that the model grid needs to be finer than about 100 m and the output interval has to be smaller than 30 minutes to fully resolve the effect of submesoscale currents on tracer transport in the nearshore region (~1 km from the shoreline) and further reducing model resolution beyond that yield no difference in particle trajectories and fates. Submesoscale currents also interacts with surface gravity waves [e.g., Romero et al. 2020], further altering the effects of both waves and submesoscale currents on plastic transport. On the other hand, it is still formidable to run a model and archive multi-year model outputs at that spatial and temporal scale for a regional ocean, as noted by Dauhaire et al. [2019]. Also, the regional-ocean scale transport is still governed by mesoscale and large-scale

circulations, the effects of submesoscale currents on the particle distributions in a regional ocean are another open research question.

All the missing dynamical processes could be straightforwardly added to the modeling framework described in Section 2. For example, to include the effect of the Stokes drift,  $(\bar{u}, \bar{v})$  will be replaced by  $(u_{ctr} + u_{st}, v_{ctr} + v_{st})$  with subscripts cir and st implying circulation and Stokes drift field from a coupled ocean-wave model. To include the effect of wave-induced mixing, diffusivity with wave-induced mixing will be used as input for  $A_{ks}$ . To include the effect of submesoscale currents, circulation fields with a spatial resolution of 100 m archived every 30 minutes will be used as input in an off-line particle tracking model, or an online Lagrangian particle tracking model, i.e., a model that concurrently simulates particle trajectories and circulation fields, can be used [e.g., Stanev and Ricker 2020; Ricker and Stanev 2020].

The study also points to the need in plastic trajectory studies that the ocean instrumentation and observing community could contribute to. As noted by the authors and pointed out by the anonymous reviewers, there are no observations that accurately follow the motion of the weakly buoyant microplastics that could be compared with the modeling results. Most ocean drifters and floats move at the ocean surface or along constant density surface in the ocean interior [e.g., Lumpkins et al. 2017]. The only instrument that could follow the turbulent motions of neutrally/weakly particles in the ocean surface boundary layer, to the authors' best knowledge, is the Lagrangian floats developed by Eric D'Asaro [e.g., D'Asaro et al. 1996]. Those floats are relatively expensive and have only been deployed at small spatial and temporal scales, therefore, have never been used to study the trajectories of microplastics. The development and deployment of low-cost weakly buoyant drifters that mimic the motion of microplastics would greatly improve our understanding of the trajectory and fate of microplastics and other weakly buoyant particulate materials in the ocean.

## Acknowledgements

The updated LTRANS code reported in this study is available through this link: https://github.com/lsuocean/LTRANS\_microplastics/. The original LTRANS code was downloaded from this link: https://northweb.hpl.umces.edu/LTRANS.htm. The hindcast solutions for circulations in the Louisiana/Texas continental shelf were downloaded from http://barataria.tamu.edu:8080/thredds/catalog.html. Some of the colormaps are from Thyng et al.

- 494 [2016]. JHL was funded by the National Science Foundation through grant OCE-1945502. JL
- was funded by the Natural Environment Research Council through grant NE/T004223/1. DK and
- 496 RH were funded by Texas General Land Office under contract 10-096-000-3927. CD was funded
- by the National Key Research Program of China (2007YFA0604100). Computations in this
- 498 study were performed using supercomputing facilities at the Louisiana State University and at
- 499 the Louisiana Optical Network Initiative. Many constructive suggestions from the three
- anonymous reviewers are greatly appreciated.

### 501 References

- Abolfazli, E., Liang, J.-H., Fan, Y., Chen, Q. J., Walker, N. D., & Liu, J. (2020). Surface gravity
- waves and their role in ocean-atmosphere coupling in the Gulf of Mexico. J. Geophys. Res.-
- 504 *Oceans*, **125**, e2018JC014820.
- Ali, A., Christensen, K. H., Breivik, Ø., Malila, M., Raj, R. P., Bertino, L., Chassignet, E. P. and
- Bakhoday-Paskyabi, M. (2019). A comparison of Langmuir turbulence parameterizations and
- key wave effects in a numerical model of the North Atlantic and Arctic oceans. *Ocean Modell.*,
- 508 137, 76-97.
- 509 Alvera-Azcárate, A., A. Barth, and R. H. Weisberg (2009), The surface circulation of the
- 510 Caribbean Sea and the Gulf of Mexico as inferred from satellite altimetry, J. Phys.
- 511 *Oceanogr.*, **39**, 640-657.
- Andrady, A. L. (2011), Microplastics in the marine environment, Mar. Pollut. Bull., 62 1596-
- 513 1605.
- Bracco, A., Liu, G., and Sun, D. (2019). Mesoscale-submesoscale interactions in the Gulf of
- 515 Mexico: from oil dispersion to climate. *Chaos Solitons Fractals*, 119, 63-72.
- 516 Chor, T., Yang, D., Meneveau, C., & Chamecki, M. (2018). A turbulence velocity scale for
- 517 predicting the fate of buoyant materials in the oceanic mixed layer. Geophys. Res. Lett., 45(21),
- 518 11-817.
- D'Asaro, E., (2014). Turbulence in the upper-ocean mixed layer. Annu. Rev. Mar. Sci., 6, 101-
- 520 115.

- 521 D'Asaro, E. A., D. M. Farmer, J. T. Osse, & G. T. Dairiki, (1996). A Lagrangian float. J. Atmos.
- 522 Oceanic Tech., **13(6)**, 1230-1246.
- Dauhajre, D. P., J. C. McWilliams, and L. Renault, (2019). Nearshore Lagrangian connectivity:
- 524 Submesoscale influence and resolution sensitivity. J. Geophys. Res.-Oceans, 124(7), 5180-5204.
- da Silva, C. E., & Castelao, R. M. (2018). Mississippi River plume variability in the Gulf of
- Mexico from SMAP and MODIS Aqua observations. J. Geophys. Res.-Oceans, 123, 6620-
- 527 6638.
- Dai, D., Qiao, F., Sulisz, W., Han, L., & Babanin, A. (2010). An experiment on the nonbreaking
- surface-wave-induced vertical mixing. J. Phys. Oceanogr., 40(9), 2180-2188.
- Davies, S. W., Strader, M. E., Kool, J. T., Kenkel, C. D., & Matz, M. V. (2017). Modeled
- differences of coral life-history traits influence the refugium potential of a remote Caribbean reef.
- 532 *Coral Reefs*, **36(3)**, 913-925.
- Dee, D. P., S. M. Uppala, A. J. Simmons, and co-authors (2011), The ERA-Interim reanalysis:
- configuration and performance of the data assimilation system. Q. J. R. Meteorol. Soc., 137, 553-
- 535 597.
- Delandmeter, P., & van Sebille, E. (2019). The Parcels v2.0 Lagrangian framework: New field
- interpolation schemes. *Geosci. Model Dev.*, 12, 3571-3584.
- 538 DiBenedetto, M. H., (2020). Non-breaking wave effects on buoyant particle distributions. *Front.*
- 539 *Mar. Sci.*, 7, 148.
- Hamlington, P. E., Van Roekel, L. P., Fox-Kemper, B., Julien, K., & Chini, G. P. (2014).
- 541 Langmuir-submesoscale interactions: Descriptive analysis of multiscale frontal spindown
- simulations. J. Phys. Oceanogr., 44(9), 2249-2272.
- Hanley, K. E., S. E. Belcher, & P.P. Sullivan, (2010). A global climatology of wind-wave
- interaction. J. Phys. Oceanogr., **40**, 1263-1282.
- Hetland R. D. and S. F. DiMarco (2012). Skill assessment of a hydrodynamic model of
- circulation over the Texas-Louisiana continental shelf. *Ocean Modell.*, **43-44**, 64-76.

- Hu, C., Nelson, J. R., Johns, E., Chen, Z., Weisberg, R. H., & Müller-Karger, F. E. (2005).
- Mississippi River water in the Florida Straits and in the Gulf stream off Georgia in summer 2004.
- 549 *Geophys. Res. Lett.*, **32**, L14606.
- Justic, D., Rabalais, N. N., Turner, R. E. (2002). Modeling the impacts of decadal changes in
- riverine nutrient fluxes on coastal eutrophication near the Mississippi River delta. Ecol. Model.,
- 552 152, 33-46.
- Kershaw, P., S. Katsuhiko, S. Lee, & D. Woodring, (2011). Plastic debris in the ocean. United
- Nations Environment Programme.
- Kobashi, D. and R. Hetland, (2020). Reproducibility and variability of sub-mesoscale frontal
- eddies over a broad, low-energy continental shelf of freshwater influence. Ocean Dynamics,
- 557 DOI:10.1007/s10236-020-01401-4.
- Kukulka, T., & Brunner, K. (2015). Passive buoyant tracers in the ocean surface boundary layer:
- 1. Influence of equilibrium wind-waves on vertical distributions. J. Geophys. Res.-Oceans,
- **120(5)**, 3837-3858.
- Kukulka, T., G. Proskurowski, S. Moret-Ferguson, D. W. Meyer, and K. L. Law, (2012), The
- effect of wind mixing on the vertical distribution of buoyant plastic debris. *Geophys. Res. Lett.*,
- 563 **39**, L07601.
- Lange, M., & van Sebille, E. (2017). Parcels v0.9: Prototyping a Lagrangian ocean analysis
- framework for the petascale age. *Geosci. Model Dev.*, 10(11), 4175-4186.
- Law, K. L. (2017), Plastics in the marine environment, Annu. Rev. Mar. Sci., 9, 205-229.
- Lebreton, L. C. M., S. D. Greer and J. C. Borerro (2012), Numerical modelling of floating debris
- in the world's oceans, *Mar. Pollut. Bull.*, **64**, 653-661.
- Li Q., B. G. Reichl, B. Fox-Kemper, A. J. Adcroft, S. E. Belcher, G. Danabasoglu, A. L. M.
- 570 Grant, S. M. Griffies, R. Hallberg, T. Hara, R. R. Harcourt, T. Kukulka, W. G. Large, J. C.
- McWilliams, B. Pearson, P. P. Sullivan, L. Van Roekel, P. Wang, Z. Zheng, (2019). Comparing
- ocean surface boundary vertical mixing schemes including Langmuir turbulence. Journal of
- 573 Advances in Modeling Earth Systems, 11, 3545-3592.

- Liang, J.-H., J. C. McWilliams, P. P. Sullivan, and B. Baschek, (2012). Large eddy simulation of
- 575 the bubbly ocean: New insights on subsurface bubble distribution and bubble-mediated gas
- 576 transfer. *J. Geophys. Res.*, 117, C04002.
- Liang, J.-H., X. Wan, K. A. Rose, P. P. Sullivan and J. C. McWilliams, (2018), Horizontal
- dispersion of buoyant materials in the ocean surface boundary layer, J. Phys. Oceanogr., 48,
- 579 2103-2125.
- Limer, B. D., J. Bloomberg, and D. M. Holstein. (2020). The Influence of Eddies on Coral
- Larval Retention in the Flower Garden Banks. *Frontiers in Marine Science*, 7, 1-16.
- Liu, B., D'Sa, E. J., & Joshi, I. (2019). Multi-decadal trends and influences on dissolved organic
- 583 carbon distribution in the Barataria Basin, Louisiana from in-situ and Landsat/MODIS
- observations. *Remote Sensing of Environment*, **228**, 183-202.
- Liu, J., Liang, J. H., McWilliams, J. C., Sullivan, P. P., Fan, Y., & Chen, Q. (2018). Effect of
- planetary rotation on oceanic surface boundary layer turbulence. J. Phys. Oceanogr., 48(9),
- 587 2057-2080.
- Liu, Y., Weisberg, R. H., Vignudelli, S., and Mitchum, G. T. (2016), Patterns of the loop current
- system and regions of sea surface height variability in the eastern Gulf of Mexico revealed by the
- self-organizing maps, J. Geophys. Res. Oceans, 121, 2347-2366.
- Liu, Y., R. H. Weisberg, C. Hu, and L. Zheng (2011), Tracking the Deepwater Horizon oil spill:
- 592 A modeling perspective, *Eos Trans. AGU*, **92(6)**, doi:10.1029/2011EO060001.
- Lumpkin, R., T. Özgökmen, & L. Centurioni, (2017). Advances in the application of surface
- 594 drifters. *Annu. Rev. Mar. Sci.*, **9**, 59-81.
- 595 Martinez-Lopez, B. and Zavala-Hidalgo, J. (2009) Seasonal and interannual variability of cross-
- shelf transports of chlorophyll in the Gulf of Mexico, *J. Mar. Syst.*, 77, 1-20.
- Maximenko, N. A., J. Hafner and P. P. Niiler, (2012), Pathways of marine debris derived from
- trajectories of Lagrangian drifters *Mar. Pollut. Bull.*, **65**, 51-62.
- McWilliams, J. C., E. Huckle, J-H. Liang, & P. P. Sullivan, (2014). Langmuir turbulence in
- 600 swell. J. Phys. Oceanogr., 44, 870-890.

- Morét-Ferguson, S., K. L. Law, G. Proskurowski, E. K. Murphy, E. E. Peacock, and C. M.
- Reddy (2010), The size, mass, and composition of plastic debris in the western North Atlantic
- 603 Ocean, Mar. Pollut. Bull., **60(10)**, 1873-1878.
- Morey, S. L., P. J. Martin, J. J. O'Brien, A. A. Wallcraft, and J. Zavala-Hidalgo, Export
- pathways for river discharged fresh water in the northern Gulf of Mexico, J. Geophys. Res.,
- 606 108(C10), 3303.
- Morton, K. W., & D. F. Mayers, (2005). Numerical solution of partial differential equations: an
- 608 introduction. Cambridge University Press.
- Nickols, K. J., Gaylord, B., & Largier, J. L. (2012). The coastal boundary layer: Predictable
- 610 current structure decreases alongshore transport and alters scales of dispersal. *Marine Ecology*
- 611 *Progress Series*, **464**, 17-34.
- North, E. W., Adams, E. E., Schlag, Z., Sherwood, C. R., He, R., Hyun, K. H., & Socolofsky, S.
- 613 A. (2011). Simulating Oil Droplet Dispersal From the Deepwater Horizon Spill With a
- 614 Lagrangian Approach. Geophysical Monograph Series, 217–226.
- North, E. W., Z. Schlag, R. R. Hood, M. Li, L. Zhong, T. Gross, and V. S. Kennedy (2008),
- Vertical swimming behavior influences the dispersal of simulated oyster larvae in a coupled
- particle-tracking and hydrodynamic model of Chesapeake Bay, Mar. Ecol. Prog. Ser., 359, 99-
- 618 115.
- Nowlin, W. D., A. E. Jochens, S. F. Dimarco, R. O. Reid, and M. K. Howard, (2005), Low-
- frequency circulation over the Texas-Louisiana continental shelf. Am. Geophys. Union, 161, 219-
- 621 240.
- Ostle, C., R. C. Thompson, D. Broughton, L. Gregory, M. Wooton, & D. G. Johns, (2019), The
- rise in ocean plastics evidenced from a 60-year time series. *Nature Communications*, **10**, 1622.
- Paris, C. B., J. Helgers, E. van Sebille, and A. Srinivasan, (2013), Connectivity modelling system:
- A probabilistic modeling tool for the multi-scale tracking of biotic and abiotic variability in the
- ocean. Environ. Modell. Software, 42, 47-54.

- Peytavin, A., B. Sainte-Rose, G. Forget, and J.-M. Campin, (2021). Ocean Plastic Assimilator
- 628 v0.1: Assimilation of Plastics Concentration Data into Lagrangian Dispersion Models, *Geosci.*
- 629 *Model Dev. Discuss.*, https://doi.org/10.5194/gmd-2020-385.
- Reisser, J., and co-authors, (2015), The vertical distribution of buoyant plastics at sea: An
- observational study in the North Atlantic Gyre. *Biogeosciences*, **12**, 1249-1256.
- Ricker, M., & E. V. Stanev, (2020). Circulation of the European northwest shelf: a Lagrangian
- 633 perspective. *Ocean Science*, **16(3)**, 637-655.
- Romero, L., D. Hypolite, & J. C. McWilliams, (2020). Submesoscale current effects on surface
- 635 waves. *Ocean Modell.*, **153**, 101662.
- 636 Schmidt, C., T. Krauth, and S. Wagner. (2017), Export of plastic debris by rivers into the sea.
- 637 Environ. Sci. Technol., 51, 21, 12246-12253.
- 638 Scircle, A., J. V. Cizdziel, K. Missling, L. Li, and A. Vianello, (2020), Single pot method for
- 639 the collection and preparation of natural water for microplastic analyses: microplastics in the
- Mississippi River system during and after historic flooding. *Envir. Tox. Chem.*, **39**, 986-995.
- 641 Shchepetkin A. F. and J. C. McWilliams (2005). The regional oceanic modelling system
- 642 (ROMS): a split-explicit, free-surface, topographically-following-coordinate oceanic model.
- 643 *Ocean Modell.*, **9**, 347-404.
- Staney, E.V., and M. Ricker, (2020) Interactions between barotropic tides and mesoscale
- processes in deep ocean and shelf regions. *Ocean Dynamics*, **70**, 713-728.
- Thyng, K. M., (2019). Deepwater horizon oil could have naturally reached Texas beaches *Mar*.
- 647 *Pollut. Bull.*, **149**, 110527.
- Thyng, K. M., C. A. Greene, R. D. Hetland, H. M. Zimmerle, & S. F. DiMarco, (2016). True
- colors of oceanography: Guidelines for effective and accurate colormap selection. *Oceanography*,
- **29(3)**, 9-13.
- Toner, K. E. (2020). Identification and Quantification of Microplastic Pollution in Water
- Samples and Four Species of Fish from the Mississippi River. Master's Thesis, Louisiana State
- 653 University.

- 654 Umlauf, L., and H. Burchard (2001). A generic length-scale equation for geophysical turbulence
- 655 models. J. Marine Res., **61**, 235-265.
- van Emmerik, T., and E. Schwarz. (2019), Plastic debris in rivers. WIREs Water, 2020;7:e1398
- van Sebille, E., M. H. England, and G. Froyland (2012), Origin, dynamics and evolution of
- ocean garbage patches from observed surface drifters, *Environ. Res. Lett.*, 7, 044040.
- van Sebille, E., C. Wilcox, L. Lebreton, N. Maximenko, B. D. Hardesty, J. A. van Francker, M.
- 660 Eriksen, D. Siegel, F. Galgani, and K. L. Law, (2015), A global inventory of small floating
- plastic debris, *Environ. Res. Lett.*, **10**, 124006.
- Van Roekel, L. P., B. Fox-Kemper, P. P. Sullivan, P. E. Hamlington, & S. R. Haney, (2012). The
- form and orientation of Langmuir cells for misaligned winds and waves. J. Geophys. Res., 117,
- 664 CO5001.
- Walker, N. D., Rouse, L. J., Fargion, G. S., & Biggs, D. C. (1994). The great flood of summer
- 666 1993: Mississippi River discharge studied. Eos, Transactions American Geophysical Union,
- **75(36)**, 409-415.
- Walker, N. D., W. J. Wiseman Jr., L. J. Rouse Jr., and A. Babin (2005), Effects of river
- discharge, wind stress, and slope eddies on circulation and satellite observed structure of the
- 670 Mississippi River plume, *J. Coastal Res.*, **216**, 1228-1244.
- Wayman, C. & Niemann, H. (2021). The fate of plastic in the ocean environment a minireview.
- 672 *Environ. Sci.: Processes Impacts*, **23**, 198-212.
- Weisberg, R. H., Zheng, L., & Liu, Y. (2017). On the movement of Deepwater Horizon oil to
- Northern Gulf beaches. *Ocean Modell.*, **111**, 81-97.
- Wichmann, D., Delandmeter, P., & van Sebille, E. (2019). Influence of near-surface currents on
- the global dispersal of marine microplastic. J. Geophys. Res. Oceans, 124(8), 6086-6096.
- Wilcox, C., B. D. Hardesty, & K. L. Law, (2020). Abundance of Floating Plastic Particles Is
- Increasing in the Western North Atlantic Ocean. *Env. Sci. Technol.*, **54**, 790-796.

- Wiseman, W. J., Rabalais, N. N., Turner, R. E., Dinnel, S. P., & MacNaughton, A. N. D. A.
- 680 (1997). Seasonal and interannual variability within the Louisiana coastal current: stratification
- and hypoxia. *Journal of Marine Systems*, **12(1-4)**, 237-248.
- Wolanski, E., & Spangol, S. (2000). Sticky waters in the Great Barrier Reef. Estuarine, Coastal
- 683 *and Shelf Science*, **50**, 27-32.
- Yang, D., B. Chen, B., M. Chamecki, M., and C. Meneveau, (2015), Oil plumes and dispersion
- 685 in Langmuir, upper-ocean turbulence: Large-eddy simulations and K-profile parameterization, J.
- 686 Geophys. Res. Oceans, 120, 4729-4759.
- Yuan, J., & Liang, J.-H. (2021). Wind-and Wave-driven Ocean Surface Boundary Layer in a
- Frontal Zone: Roles of Submesoscale Eddies and Ekman-Stokes Transport. J. Phys. Oceanogr.,
- 689 DOI:/10.1175/JPO-D-20-0270.1
- 690 Zavala-Hidalgo, J., Morey, S. L., and O'Brien, J. J. (2003). Seasonal circulation on the western
- shelf of the Gulf of Mexico using a high-resolution numerical model, J. Geophys. Res., 108,
- 692 3389.

704

705

- 693 Zhang, X., Hetland, R. D., Marta-Almeida, M., & DiMarco, S. F. (2012a). A numerical
- 694 investigation of the Mississippi and Atchafalaya freshwater transport, filling and flushing times
- on the Texas-Louisiana Shelf. J. Geophys. Res.-Oceans, 117(C11).
- Zhang, X., M. Marta-Almeida, and R. D. Hetland (2012b). A high-resolution pre-operational
- 697 forecast model of circulation on the Texas-Louisiana continental shelf and slope, Journal of
- 698 *Operational Oceanography*, **5(1)**, 19-34.
- 699 Zhang, Z., R. Hetland, & X. Zhang, (2014). Wind-modulated buoyancy circulation over the
- Texas-Louisiana shelf. J. Geophys. Res.-Oceans, 119(9), 5705-5723.
- 701 Zhong, Y., A. Bracco, and T. A. Villareal (2012), Pattern formation at the ocean surface:
- Sargassum distribution and the role of the eddy field, *Limnol. Oceanogr.*, **2**, 12-27.

710 Table 1. Statistics of riverborne plastics over the Louisiana/Texas continental shelf

Origin	w <sub>b</sub> [mm/s]	Distance [km]	Time [day]	Speed [km/day]	Beaching [%]	Beaching west of LA [%]	Beaching @ LA [%]	East of Origin [%]
Missis	8	626.9	31.3	24.5	62.7	18.5	44.2	26.9
sippi	10	674.5	34.6	23.9	63.6	21.8	41.8	26.7
River	0.5	1043.2	57.4	22.1	52.6	26.0	26.5	28.2
Atchaf	$\infty$	417.4	31.7	14.5	88.1	18.2	69.9	22.5
alaya	10	420.6	32.3	14.1	88.6	19.7	68.9	22.1
River	0.5	690.9	49.2	14.3	80.9	24.0	56.9	21.3

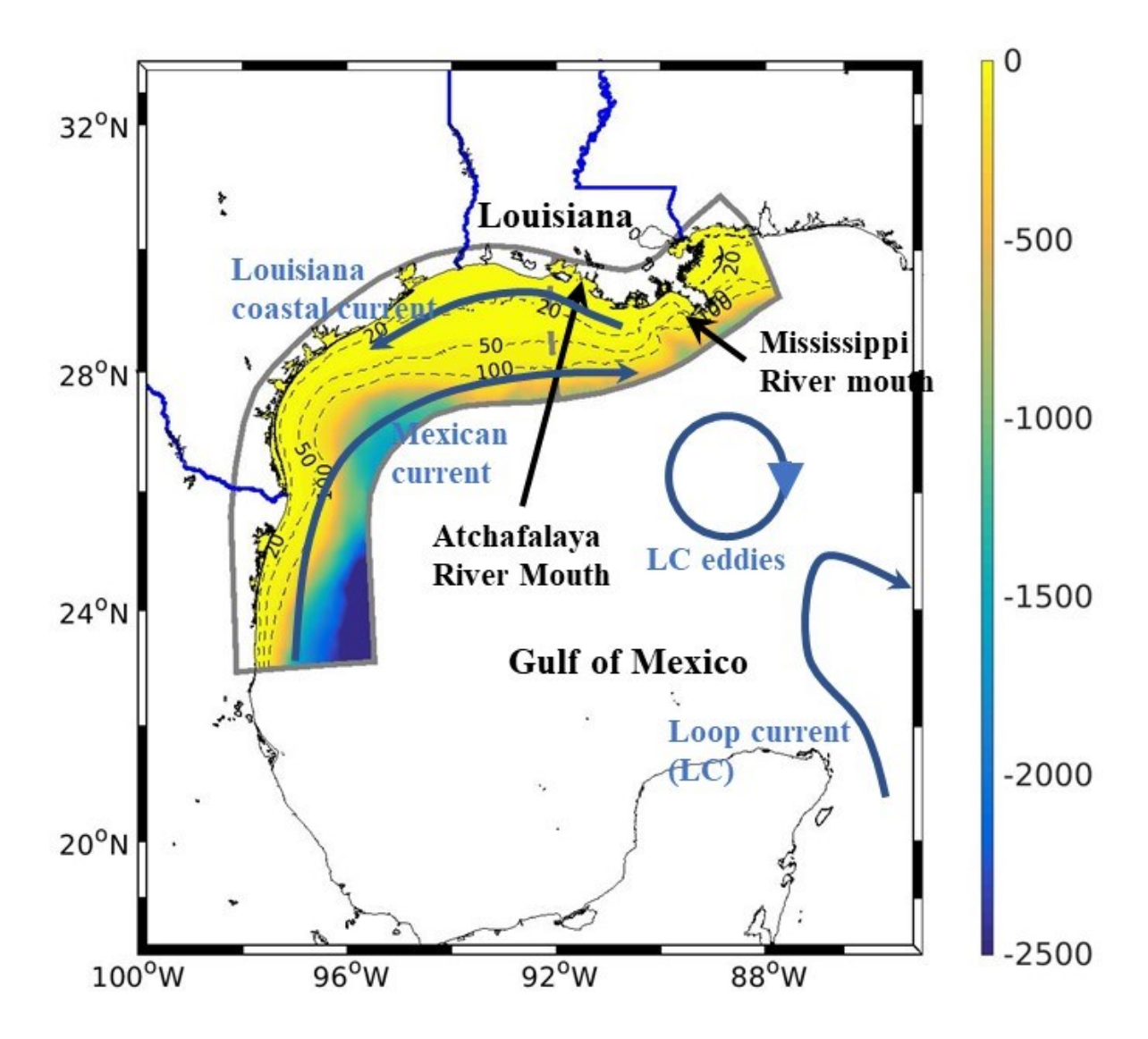


Figure 1. The geographic location of the simulation domain (solid gray lines) and regional circulations (thick solid blue lines) including the Louisiana coastal current (LCC), the Mexican current, the Loop current and the Loop current eddies. The direction of the LCC in the schematic is for non-summer months. The current reverses its direction during summer months. Both the colormap and the contours are for water depth. The dashed gray line is the location of the transect shown in Fig. 6.

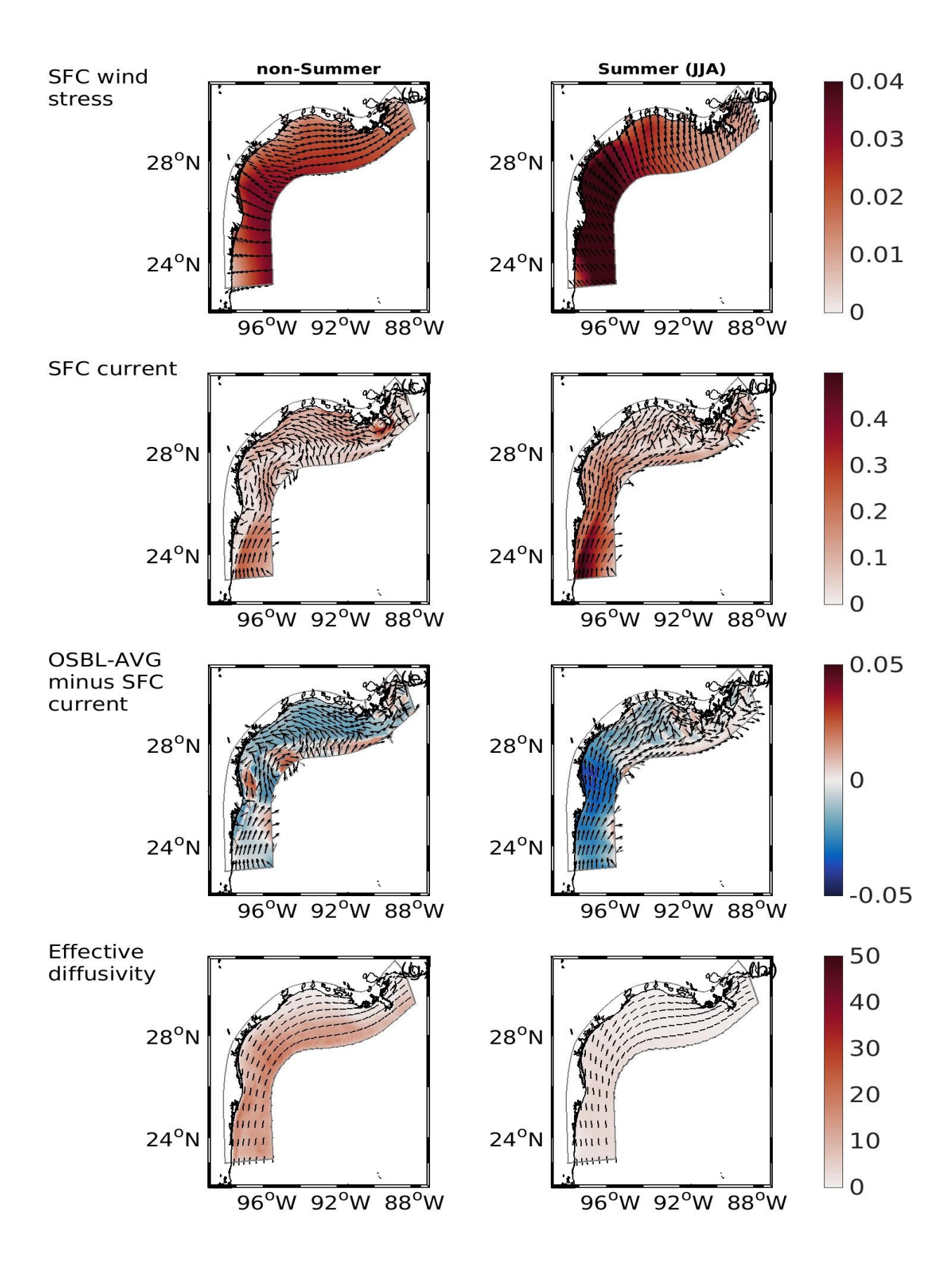


Figure 2. The upper two panels are the maps of surface wind stress (N/m²) in (a) non-summer (months other than June, July and August) and (b) June, July and August (JJA). Colormap is the magnitude and arrows indicate the direction. The panels in the second row are maps of surface current (m/s) in (c) non-summer and (d) JJA. The panels in the second row are the maps of horizontal currents averaged over the ocean surface boundary layer and the surface currents (m/s) in (e) non-summer and (f) JJA. Colormap is the magnitude difference between the OSBL-averaged and the surface currents. The black arrows indicate the direction of the surface currents and the gray arrows indicate the direction of the OSBL-averaged currents. The bottom two panels are the maps of effective horizontal diffusivity due to vertical shear of horizontal currents in the ocean surface boundary layer (m²/s) in (g) non-summer and (h) JJA. The colormap is for magnitude while the ellipses are for the direction. The diffusivity is highly anisotropic.

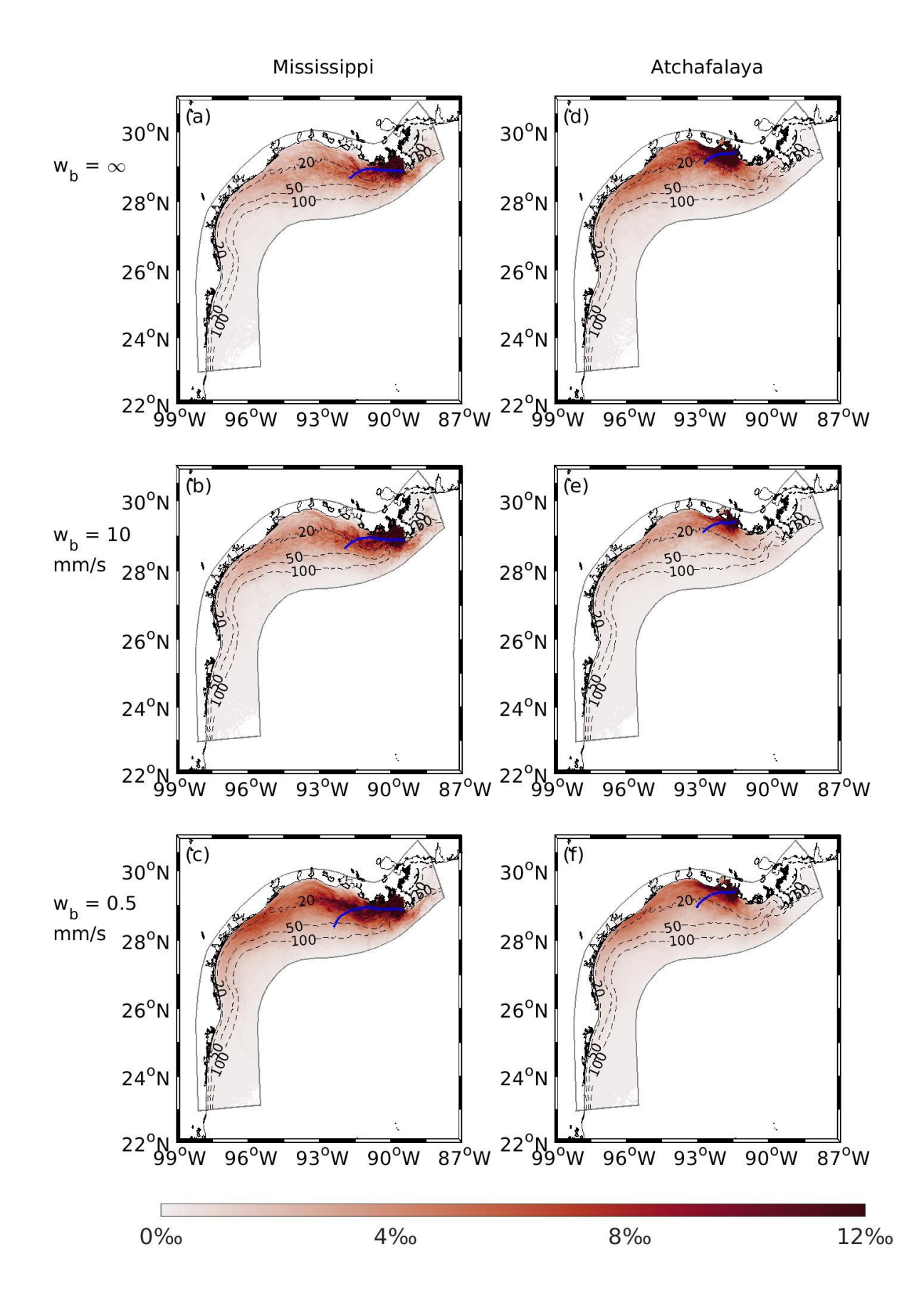


Figure 3. The annually averaged trajectories (solid blue lines) and heat maps (color, probability per km<sup>2</sup>) of plastics from the Mississippi and the Atchafalaya Rivers. Panels (a) to (b) are for those from the Mississippi River; panels (d) to (f) are for those from the Atchafalaya River; panels (a) and (d) are for floating particles; panels (b) and (e) are for those with a rising speed of 10 mm/s; and panels (c) and (f) are for those with a rising speed of 0.5 mm/s. Dashed lines are contours of bottom bathymetry.

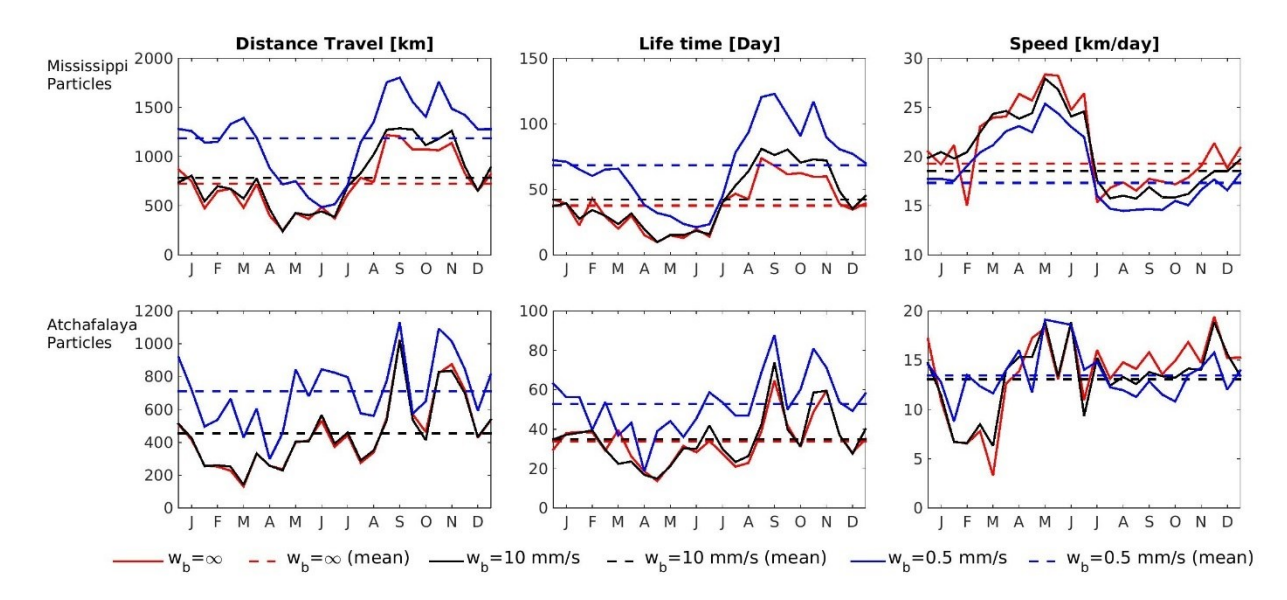


Figure 4. The monthly climatology of particle transit distance (left column), particle lifetime (middle column) and average particle speed (right column) for discharge from the Mississippi River (upper row) and the Atchafalaya River (lower row). The x-axis is the particle discharge time.

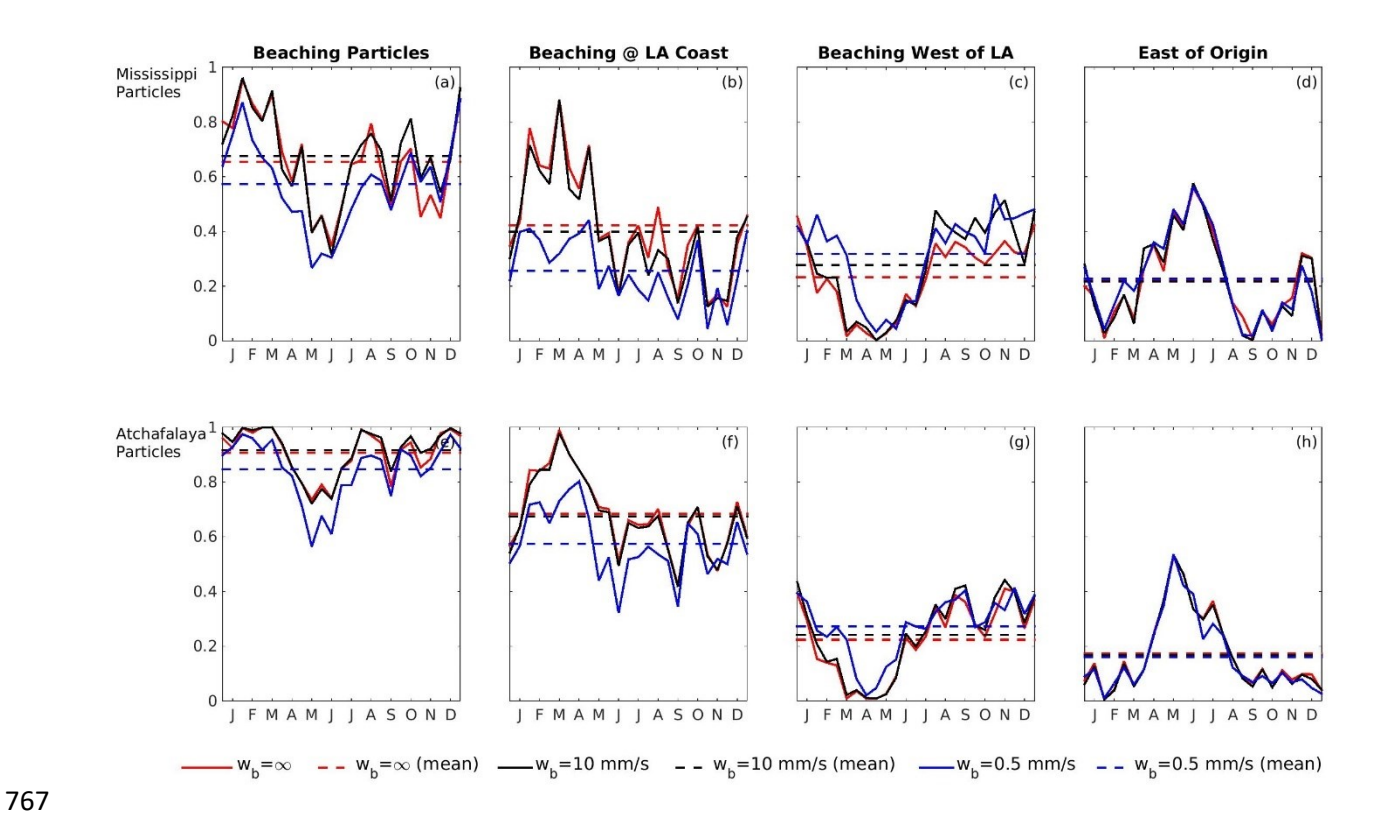


Figure 5. The monthly climatology for the fractions of particles that stop at the land boundary of the domain (first column), those that stop at the land boundaries of Louisiana (second column); those that stop at the land boundaries east of Louisiana (third column); and those that stop east of their origin (fourth column). The upper panels are for particles from the Mississippi River and the lower panels are for particles from the Atchafalaya River.

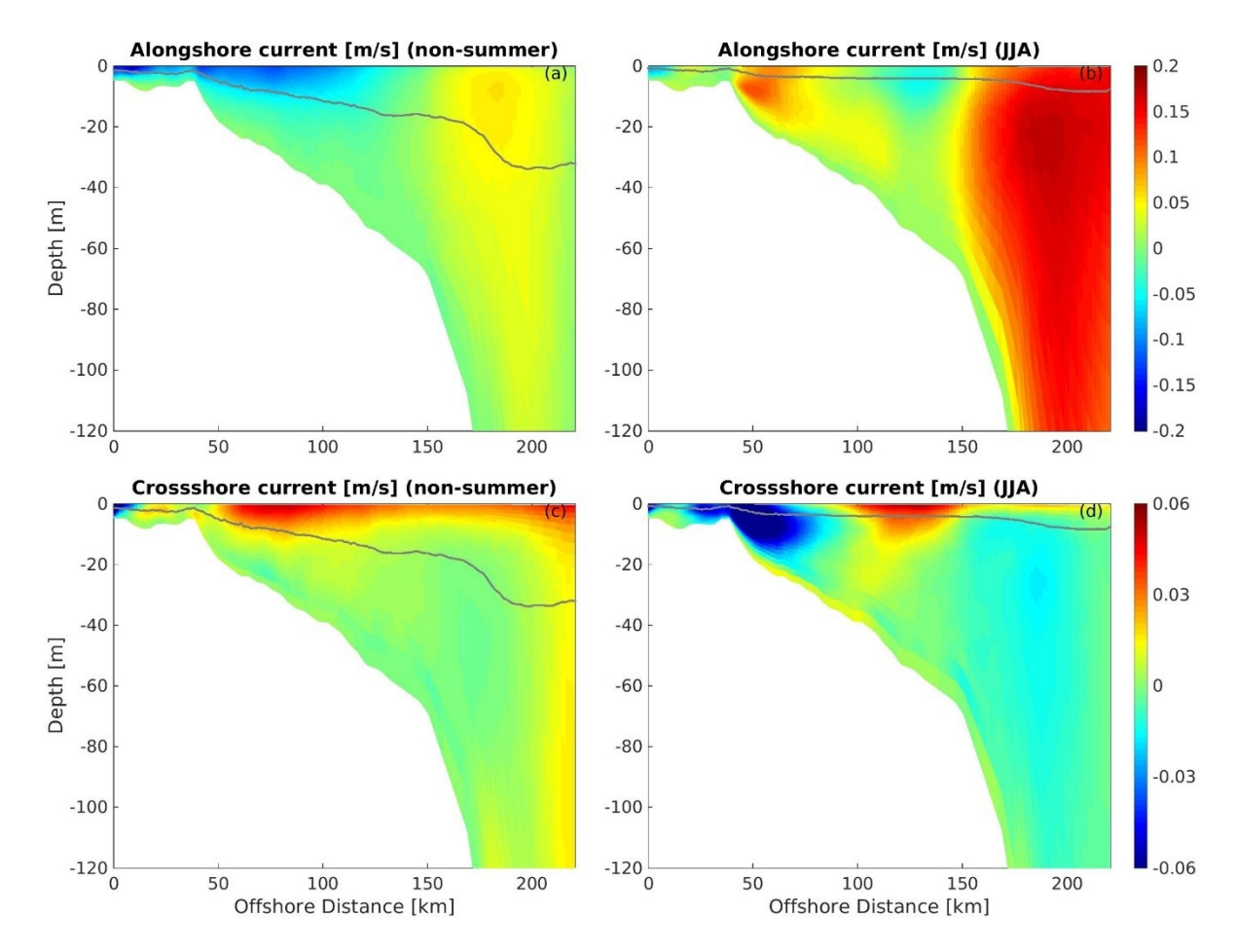


Figure 6. Along-shore (upper row) and cross-shore current (lower row) along the transect denoted by the dashed gray line in Fig. 1. Positive is for eastward along-shore current and shoreward cross-shore current, respectively. The solid grey line is the depth of the ocean surface boundary layer. The left column are averages over non-summer months, i.e., months except June, July, and August (JJA). The right column are averages over summer months (JJA).

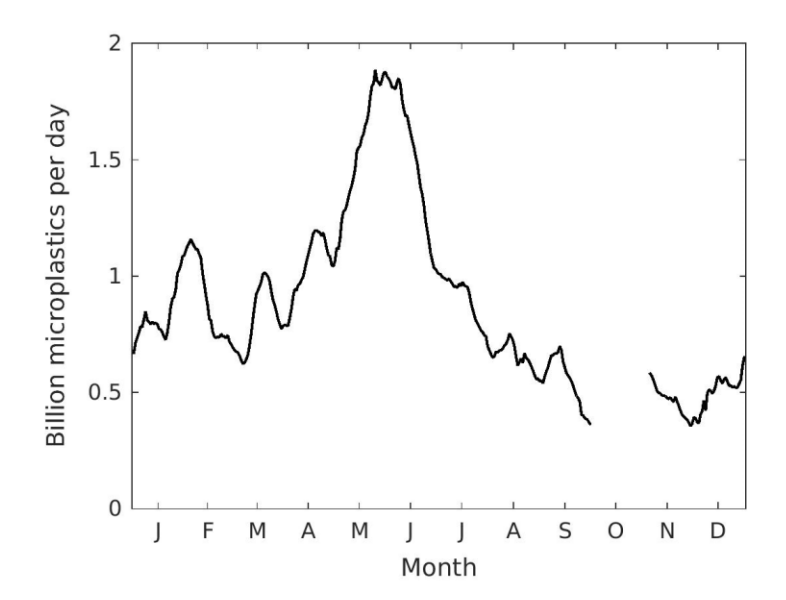


Figure 7. Monthly climatology of plastic flux in the Mississippi River. The measurement was taken from November 2016 to September 2017. Details of the measurement are in Toner [2020].